Efficient combustion parameter prediction and performance optimization for a diesel engine with a low throughput combustion model

Efficient combustion parameter prediction and performance optimization for a diesel engine with a low throughput combustion model

Matías Fernando Benedetto[a], Stefano Berrone[a], Stefano Scialò[a,*]

[a] *Dipartimento di Scienze Matematiche, Politecnico di Torino, Corso Duca degli Abruzzi 24, 10129 Torino, Italy.*

Abstract

In this work, an efficient implementation of a redzero-dimensional model is described for the estimation of key engine parameters for combustion control in compression-ignition engines. The direct problems of the estimation of the angle of 50% of fuel mass fraction burnt (MFB50) and of the mean effective pressure (IMEP) are addressed as well as the inverse problems of determining optimal start of injection (SOI) timing for target values of MFB50 and IMEP. The main focus is on the computational cost of the algorithms proposed, designed in order to keep the number of operations as low as possible without compromising the applicability of the methods to different engine configurations and operation points. red Execution time of the order of few milliseconds are achieved for parameters prediction and of the order of one tenth of a second for the optimization problems, such that an implementation in engine ECU for model-based control purposes can be envisaged.

Keywords: Model-based combustion control in CI engines, Diesel combustion modelling, Predictive models for combustion, Numerical simulation of combustion, Numerical optimization

1. Introduction

The increasing interest towards environmentally friendly automotive compression ignition (CI) engines is stimulating the development of unconventional combustion strategies that require sophisticated redand reliable sim-

*Corresponding author

Email addresses: matias.benedetto@polito.it (Matías Fernando Benedetto), stefano.berrone@polito.it (Stefano Berrone), stefano.scialo@polito.it (Stefano Scialò)

ulation tools for the description of the combustion phase at different engine operating points. A variety of models is available in the literature ranging from simple zero-dimensional models to full CFD simulations of the combustion in the cylinder, [1, 2, 3, 4, 5, 6, 7, 8, 9, 10, 11, 12, 13, 14, 15, 16, 17]. Clearly a trade off between the accuracy of the model and the response time is required. Sophisticated control techniques of the combustion phase are also crucial for high thermal efficiencies and low emissions in diesel engines [18, 19, 20, 21, 22, 23, 24, 25, 26, 27, 28, 29, 30, 31, 32]. Model-based combustion control strategies allow to predict in advance key engine combustion parameters such as the MFB50 (i.e. the crank angle at which 50% of fuel is burnt), the peak pressure, $p_{\max}$ and the Indicated Mean Effective Pressure, IMEP.

The MFB50 is a parameter commonly used to characterize combustion phasing and to control the efficiency of the combustion, the emission levels and noise, [31, 24, 7, 33, 34, 35, 36], while the IMEP correlates the injected chemical energy to the torque requirement.

Model based control strategies redare suitable for real-time selection of main engine parameters in order to meet specific target values of MFB50 and IMEP. In this context well calibrated zero-dimensional models are often preferred to more complex models, since these models use simplified approaches to simulate the release of chemical energy, the evolution of the pressure and of chemical reactions in the combustion chamber. Moreover these models can be more easily inverted, i.e. it is possible to derive inverse functions that express the required targets (MFB50 and IMEP) as a function of the engine operation parameters [37, 38, 26, 27, 28, 29, 39]. In fact zero-dimensional models rely on a limited set of parameters calibrated for different engine applications thus combining good reliability, simplicity and a low computational effort and allow for a real-time response [16, 25, 31, 30]. However efficient implementation techniques, capable of drastically reducing the computational cost of the simulations are still necessary to effectively implement model based control strategies in current technology engine ECUs. Inverse models, in general, would involve an iterative optimization process requiring the evaluation of the predictive model at each iteration, such that even lightweight implementations could require excessive time for a real-time response.

In the present work we obtain an analytical solution of the approximated heat release rate, as described in red[26, 31], which is then used for the prediction of the MFB50 combustion parameter. A lean implementation for the numerical resolution of the model for the prediction of the IMEP is also proposed. Furthermore an efficient solution strategy is obtained for the inverse problem of estimating the Start of Injection (SOI) angle capable of deliver-

ing a target MFB50, according to the model considered. We also address the inverse problem that concerns the evaluation of the SOI angle that maximize the IMEP parameter, highlighting the strategies for an effective implementation. redAt the cost of a larger computational time, the method can be extended in order to incorporate the prediction and the optimization of pollutant emission, via some models for chemical reactions in the combustion chamber, [28, 29].

redModel based control strategies have the potential of achieving high efficiencies in the operation of diesel engine, since can predict and avoid the occurrence of inefficient combustion cycles, thus overcoming the limitations of closed-loop control techniques. The equations reported and the algorithms designed in the present work allow to predict the MFB50 and the IMEP in different operating conditions with a very limited computational effort and time, which is crucial for the success of model based control since the limited computational power available in the engine ECUs requires very lean implementations in order to provide a response in real-time.

2. Model

The present work provides an implementation of the low throughput model presented in red[26, 30]. We focus on a lean implementation with a very low computational cost. In this first Section the analytical model is briefly reported.

The calculation of the released chemical energy Q_{ch} in the combustion chamber is based on the accumulated fuel mass approach, also taking into account the effect of ignition delay through an ignition-delay correlated parameter τ, and considering the contribute of multiple injection pulses. All the equations will be presented here choosing the connection rod angle θ as the independent variable; expressions in terms of time t can be obtained through a simple affine transformation. For each injection pulse j we have:

$$\frac{dQ_{\mathrm{ch}}}{d\theta} = K_j[Q_{\mathrm{fuel}}(\theta - \tau_j) - Q_{\mathrm{ch}}(\theta)] \tag{2.1}$$

where, red being θ_{soi} and θ_{eoi} the start of injection (SOI) and end of injection (EOI) angle, respectively, Q_{fuel} is defined as:

$$Q_{\mathrm{fuel}} = \int_{\theta_{\mathrm{soi}}}^{\theta} \dot{m}(\theta) H_{\mathrm{i}} d\theta \qquad \theta \leq \theta_{\mathrm{eoi}} \tag{2.2}$$

$$Q_{\mathrm{fuel}} = \int_{\theta_{\mathrm{soi}}}^{\theta_{\mathrm{eoi}}} \dot{m}(\theta) H_{\mathrm{i}} d\theta \qquad \theta > \theta_{\mathrm{eoi}} \tag{2.3}$$

and $Q_{\rm ch} = \sum_{j=1}^{n} Q_{\rm ch}$. redIn the previous expressions $\dot{m}(\theta)$ is the fuel injection rate and $H_{\rm i}$ is the lower heating value of the fuel. The model parameters K_j and τ_j are appropriately calibrated to obtain good agreement with experimental data. The parameters K_j are constant, whereas, regarding the parameters τ_j, two different approaches are used: in a first case also τ_j is considered constant, or alternatively this parameter can be correlated to $\theta_{\rm soi}$ (or equivalently to the SOI time $t_{\rm soi,j}$) through the following expressions:

$$\tau_{\rm pil} = A e^{-B\rho_a(\theta_{\rm soi})}, \tag{2.4}$$

for all pilot injections and, for the main injection:

$$\tau_{\rm main} = \rho_a(\theta_{\rm soi}) e^{C/T_a(\theta_{\rm soi})} f(O, p_f, n, q_f), \tag{2.5}$$

being A, B, C some positive constants and the function $f(O, p, n, q_f)$ depending on the relative concentration of oxygen (O), injection pressure p_f, engine speed n and injected fuel quantity q_f. The quantities $\rho_a(\theta)$ and $T_a(\theta)$ are defined as:

$$\begin{aligned} \rho_a(\theta) &= \frac{MAP}{RT_{\rm int}} \frac{V_{\rm BDC}}{V(\theta)} \\ T_a(\theta) &= T_{\rm int} \left(\frac{V_{\rm BDC}}{V(\theta)} \right)^{(m-1)} \end{aligned}$$

with $V(\theta)$ the combustion chamber volume, $V_{\rm BDC}$ the volume at bottom dead centre, MAP the intake manifold air pressure and $T_{\rm int}$ the intake temperature, and m the exponent of the polytropic expansion law. redThe experimental law for $\tau_{\rm pil}$ is calibrated in the range 316.2-362.7 CA with a correlation coefficient of 0.951, while the law for $\tau_{\rm main}$ in the range 355.5-367.7 CA with a correlation coefficient of 0.926 [30].

Starting from $Q_{\rm ch}$, an estimation of the charge net energy, $Q_{\rm net}$, red at start of combustion (SOC) is achieved by multiplying $Q_{\rm ch}$ by a certain parameter depending on the heat exchanged with the engine walls red, $\Delta Q_{\rm ht,glob}$, and then red $Q_{\rm net}$ at SOI is obtained subtracting the energy lost due to fuel evaporation. Namely,

$$Q_{\rm net}^{\rm SOC} = Q_{\rm ch} \frac{m_{\rm f,inj} H_{\rm i} - \Delta Q_{\rm ht,glob}}{q_{\rm f,inj} H_{\rm i}} \tag{2.6}$$

$$Q_{\rm net}^{\rm SOI} = Q_{\rm net}^{\rm SOC} - \Delta Q_{\rm f,evap}, \tag{2.7}$$

red where $q_{\rm f,inj}$ the total injected fuel quantity. A parabolic function is used to complete the curve of $Q_{\rm net}$ between SOI and SOC with C^1 continuity at

$Q_{\text{net}}^{\text{SOC}}$.

The prediction of the pressure trace is obtained starting from the derivative of Q_{net}, dQ_{net} through the resolution of the differential equation

$$dp = \frac{\gamma - 1}{V}(dQ_{\text{net}} - \frac{\gamma}{\gamma - 1}pdV). \tag{2.8}$$

The complete pressure profile can be obtained adding polytropic expansion curves between intake valve closing (IVC) and SOI and between redend of combustion (EOC) and exhaust valve opening (EVO). Between EVO and IVC of the following cycle the pressure is constant and equal to intake pressure.

3. Prediction of parameters

The primary interest of the present work is to accurately and effectively calculate key combustion parameters that are important in engine control, according to the model reported in the previous Section. Procedures to obtain the peak firing pressure ($p_{\max}$), the angle of 50% fuel mass fraction burnt (MFB50) and the Indicated Mean Effective Pressure (IMEP) are described.

The numerical solutions developed here have great versatility, in the sense that the computational cost can be beforehand determined in relation to the desired accuracy, such that it is possible to have a thorough control over the computational time and accuracy with a trade off between the two. The developed numerical tools and relative results are shown performing the prediction of the aforementioned combustion parameters for several operation points for the *General Motors 2.0L A20DTR*, see Table 3.1. red Table 3.2 reports the correlation coefficients R_{corr} between the experimental data and model results for MFB50, IMEP and $p_{\max}$, and full details on the validation of the model considered can be found in [26, 27, 28, 29, 30].

If the injection profile can be approximated with a triangular shape, it is possible to analytically solve the differential equation governing the chemical energy release rate, Q_{ch}. Computations are reported in Appendix A. redIn Figure 3.1 for a rotational speed of 1500 rpm and 5 bar of brake mean effective pressure (labelled 1500x5), the triangular profile compared with an experimental injection profile is shown. The curves of the functions for Q_{net} and its derivative can be obtained analytically as well and are reported in Figures 3.2-3.3 redat the 1500x5 engine point.

3.1. MFB50

The MFB50 angle is defined as the crank angle for which 50% of the fuel mass fraction has burnt, red or, since it is assumed that all the injected fuel

Table 3.1: Data for the GM 2.0LA20DTR engine

Engine Type	2.0L “Twin-Stage” Euro V
Displacement	1956 cm^3
Bore × stroke	83.0 mm × 90.4 mm
Conrod length	145 mm
Compression ratio	16.5
Valves per cylinder	4
Turbocharger	Twin-stage with valve actuators and WG
Fuel injection system	Common Rail 2000 bar piezo
Specific power and torque	71 kW/l - 205 Nm/l

Table 3.2: Correlation coefficients for model predicted quantities

	MFB50	IMEP	$p_{\max}$
R_{corr}	0.92	0.99	0.99

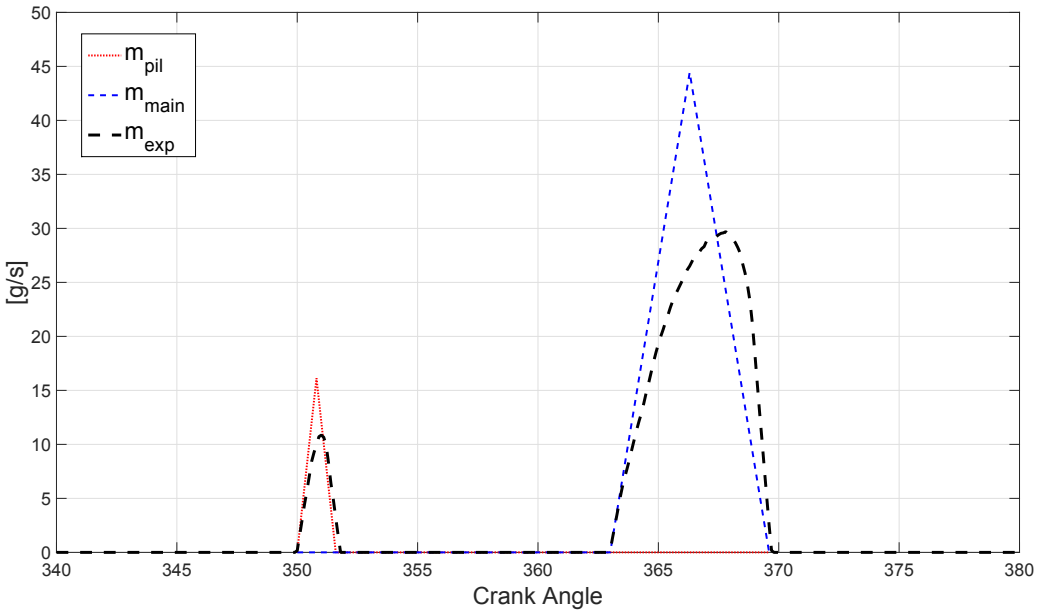

Figure 3.1: Pilot and main injections @1500x5 engine point

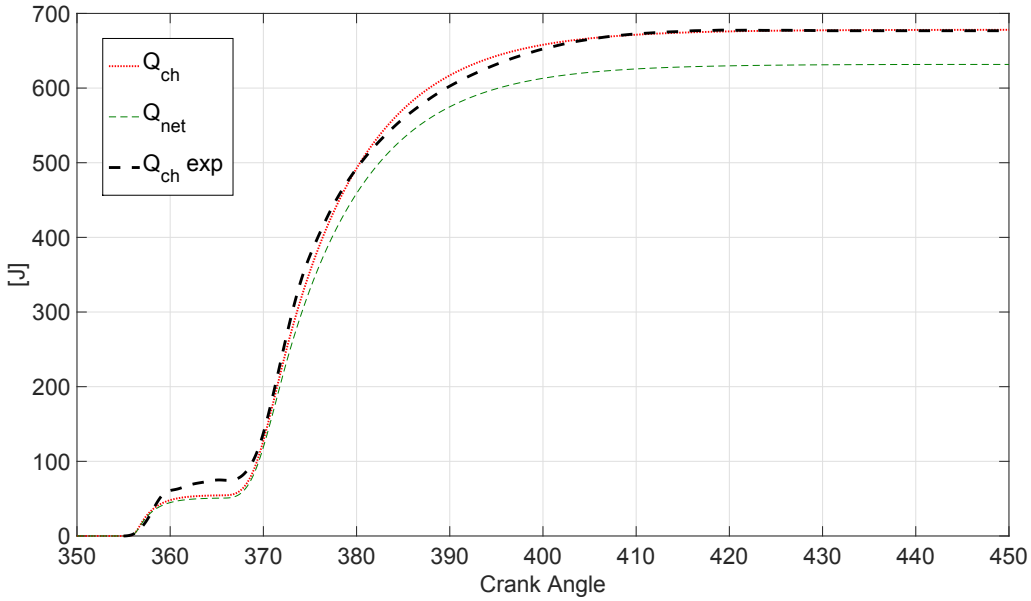

Figure 3.2: Q_{ch}, and Q_{net} @1500x5 engine point

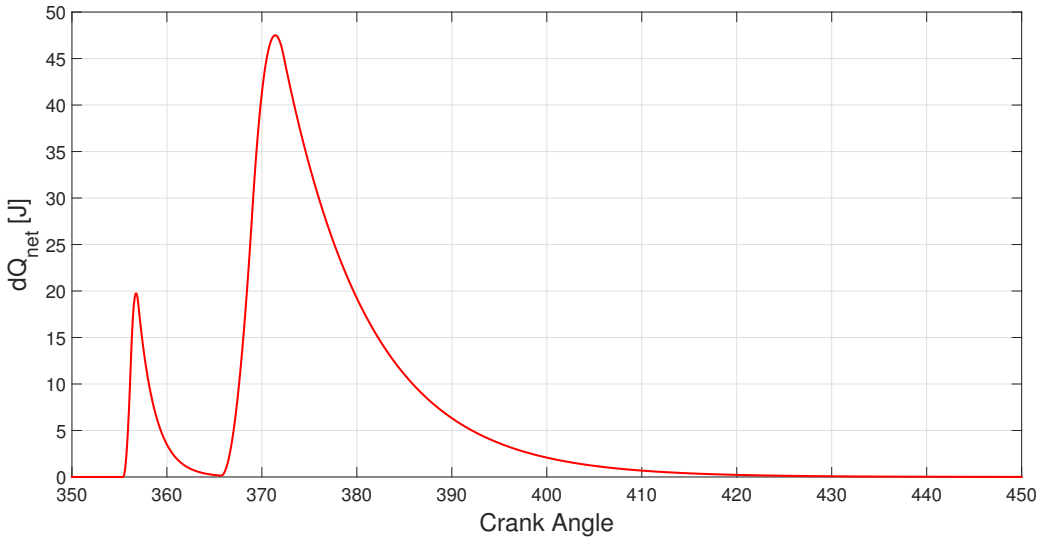

Figure 3.3: dQ_{net} @1500x5 engine point

$q_{\mathrm{f,inj}}$ is burned, it can be obtained from the Q_{ch} function solving the following problem: *find θ such that*

$$Q_{\mathrm{ch}}(\theta) = \frac{Q_{\mathrm{ch,max}}}{2} = \frac{q_{\mathrm{f,inj}} H_{\mathrm{i}}}{2},$$

or, equivalently, find the zeros of

$$f(\theta) := Q_{\mathrm{ch}}(\theta) - \frac{q_{\mathrm{f,inj}} H_{\mathrm{i}}}{2}.$$

Using the analytical expression for Q_{ch}, the roots of $f(\theta)$ can be easily found for any given accuracy using a combined Newton-Raphson/bisection method. When possible, i.e. when convergence of the method is assured, a Newton-Raphson step is performed. Otherwise a bisection step is performed. The Newton-Raphson method has a quadratic convergence rate and is computationally inexpensive, requiring only two function evaluations at each step, since also the derivative of the objective function is known analytically. On the other hand, since the curve of Q_{ch} is almost constant in certain zones of the domain, convergence of the method is not guaranteed. In these areas the bisection method is used since its convergence is assured, only requiring the continuity of Q_{ch}.

3.2. Pressure profile and Peak firing pressure

We deal now with the resolution of the differential equation that determines the pressure profile p. This can be done numerically and different choices are available for the discretization of the computational domain, for example equally spaced nodes, obtained spacing with a constant time/angle step, or non equally spaced nodes, as Gaussian quadrature nodes redor adaptive discretizations. The second choice has the advantage that an efficient quadrature rule can be used in conjunction with Gaussian nodes and weights, so the computational cost for determining the pressure profile and subsequently the integration to obtain the IMEP is optimized, and it is possible to control the accuracy level of both the resolution of the differential equation and of the numerical integration simultaneously. Gauss-Lobatto nodes are chosen in this context since these nodes include the endpoints of the intervals. The differential equation is solved with a second order method, the Heun method. As mentioned the complete pressure profile is obtained adding the pressure trace given by a polytropic law before SOC and after EOC and setting the chamber pressure equal to ambient pressure after redexhaust valve opening (EVO). The pressure profile is reported in Figure 3.4 redat 1500x5, along with the experimental pressure trace. It can be seen

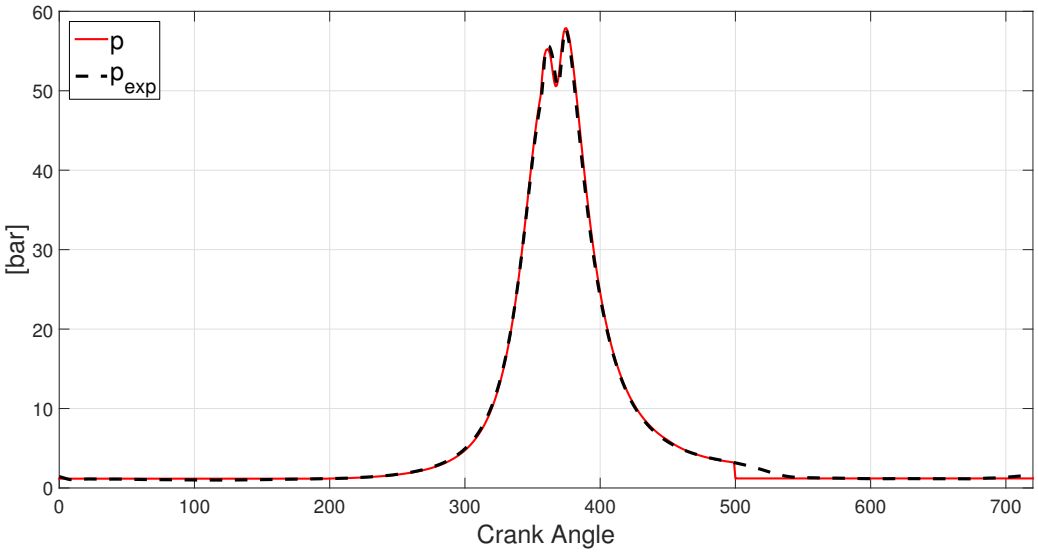

Figure 3.4: Complete pressure profile @1500x5

that there is a small jump at EVO, deriving from the simplifying assumptions of the model. However the impact of this approximation can be safely neglected for the computation of the IMEP, as shown by the good agreement with experimental data (see Table 3.2 and [29]).

The determination of the peak firing pressure is straightforward after the pressure profile is known. However it should be noted that, in theory, depending on the SOI time/angle the peak of the pressure might be reached during the polytropic compression before the combustion phase, or during the combustion phase. This depends on the volume law of the engine cylinder and for the model considered. red In this case the maximum pressure value of the polytropic curve is attained for $\theta = 360°$. Let us call p_{sol} the array of size n containing the computed value of pressure between SOC and EOC, and let us denote by $poly_E(\theta)$ and $poly_C(\theta)$ the polytropic expansion and compression phases respectively. Then the peak firing pressure is given by:

$$
\begin{aligned}
p_{\max} &= \max_{i=1,\dots,n} \{p_{\text{sol}}(i), poly_E(360)\} && \text{if EOC} < 360 \\
p_{\max} &= \max_{i=1,\dots,n} \{p_{\text{sol}}(i)\} && \text{if SOC} < 360 < \text{EOC} \\
p_{\max} &= \max_{i=1,\dots,n} \{p_{\text{sol}}(i), poly_C(360)\} && \text{if SOC} \geq 360.
\end{aligned}
$$

The accuracy and the cost for determining the peak firing pressure depends on the accuracy chosen for the resolution of the differential equation that

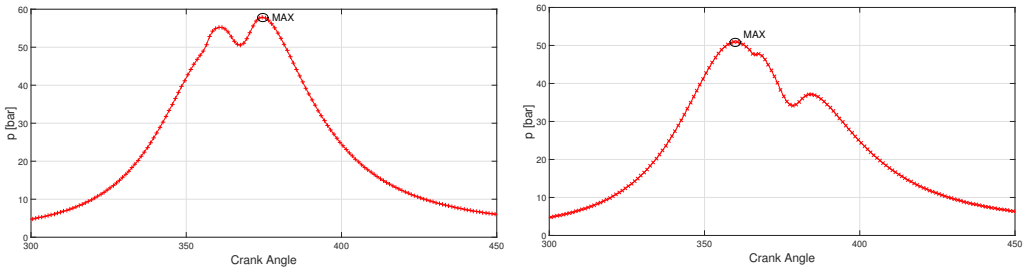

Figure 3.5: Left: $p_{\max}$ reached during combustion. Right: $p_{\max}$ is the value of the polytropic curve at 360°.

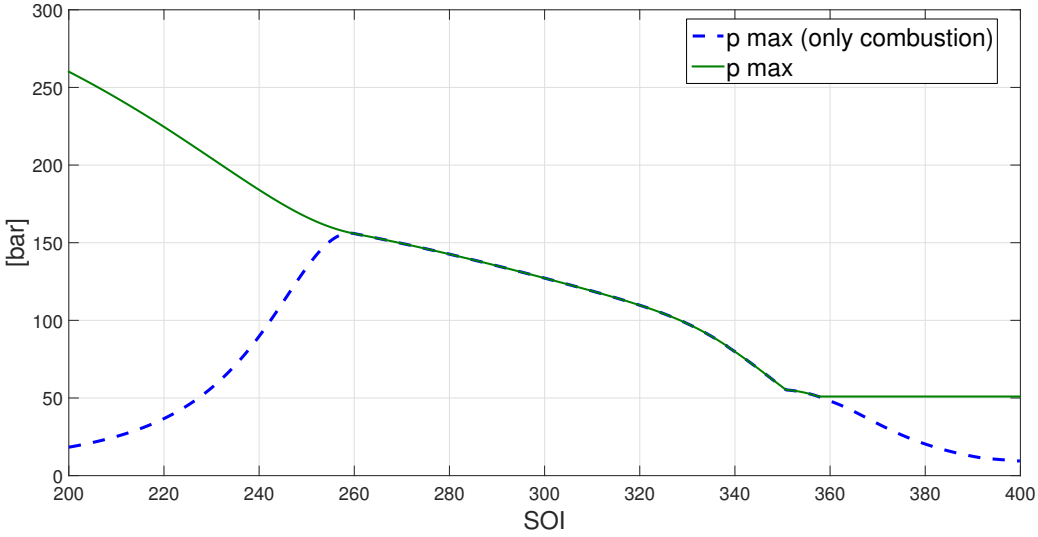

Figure 3.6: The peak firing pressure $p_{\max}$ for different values of SOI, taking into account only combustion (blue curve) or the absolute maximum(green curve),

defines p. Figure 3.5 shows the value of $p_{\max}$ for certain values of SOI and Figure 3.6 shows how that value changes with SOI.

3.3. IMEP

The Indicated Mean Effective Pressure (IMEP) is defined as:

$$\text{IMEP} = \frac{1}{\text{D}} \int_0^{720} p(\theta) \frac{dV}{d\theta} d\theta,$$

red where D is the unitary displacement. As already mentioned, since the pressure trace between SOC and EOC is known in the selected quadrature nodes the numerical integration can be straightforwardly performed. Outside the interval SOC-EOC, where the pressure is governed by a polytropic

law, integration can be performed inexpensively using the same quadrature law, but requiring few function evaluations in the selected nodes. We are interested in obtaining an accurate solution with the least amount of effort. In order to do so, we split the domain into four regions and integrate numerically on each one separately. With reference to Figure 3.7, it is possible to identify the four regions in this way: a first region between IVC and SOC, a second region between SOC and EOC, a third region between EOC and EVO and a fourth region between EVO and IVC. In the region between EVO and IVC the pressure is constant, such that no numerical integration is required, being the IMEP of this zone given by $V(\theta_{\mathrm{EVO}}) - V(\theta_{\mathrm{IVC}})$. We divide each of the remaining three regions into I macro-intervals and each macro-interval into $N+1$ sub-intervals determined by N internal Gauss-Lobatto nodes, such that the total number of nodes in each of the three regions is $I(N+1)+1$. In the example reported in Figure 3.7, red corresponding to the engine point 1500x5, the region between IVC and SOC is split into $I = 1$ macro-interval with six sub-intervals ($N = 5$ Gauss-Lobatto internal nodes and seven total Gauss-Lobatto nodes), whereas the region between EOC and EVO has one macro-interval with three sub-intervals. The region between SOC and EOC (the most important one, because it is where combustion happens) inherits the subintervals and nodes that were determined when the ODE for p was solved. In this case we have four macro-intervals for a total of thirteen nodes. It is interesting to notice that the proposed approach is capable of coupling the accuracy of the numerical resolution of the ODE (2.8) to the accuracy of the numerical integration. In fact it is useless to use a quadrature law very precise if the input data suffer from lack of accuracy, or vice versa. Increasing the number of macro-intervals and/or of sub-intervals the accuracy of both resolution and integration of the pressure profile are improved, at the cost of an increasing number of computations. However the computational cost can be pre-determined and selected according to the required level of accuracy. Several numerical results have been performed, with different schemes of discretization labelled with capital letters from A to E. The total number of nodes increases from scheme A to scheme E. Figure 3.8 shows the computation of the pressure profile between SOC and EOC for the different discretization schemes with the Heun method redalong with a reference solution and the experimental curve, p_{exp}. It is possible to notice that, except the scheme with the lower number of nodes, all the curves are well overlapped to the reference solution. red For the sake of our investigation the reference solution is a very accurate solution provided by the considered method, i.e. obtained with a very large number of nodes. This is because we aim at developing a lean implementation of the model that does not compromise its accuracy. In Table 3.3 details of IMEP computation in the four identified

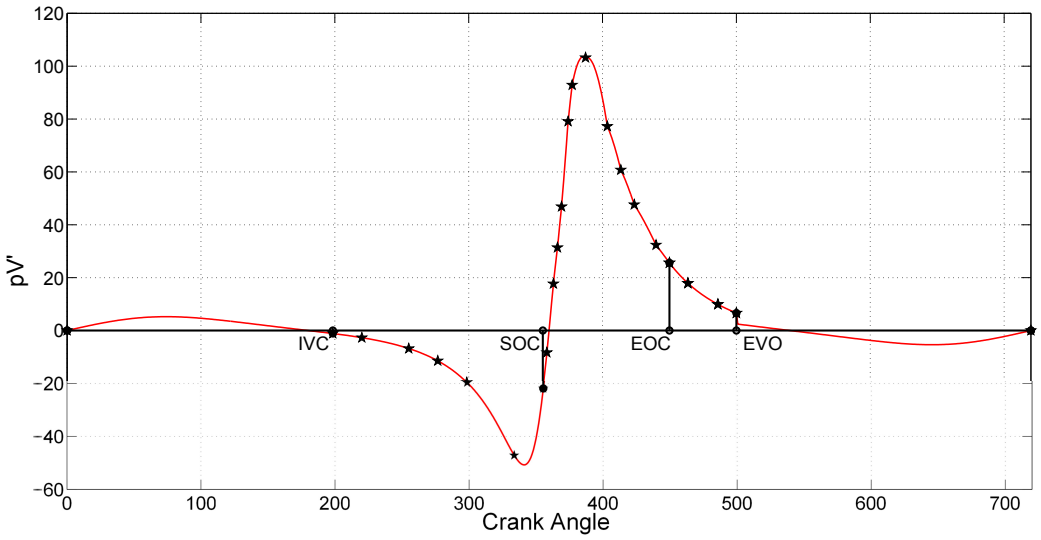

Figure 3.7: Subdivision of the domain for numerical integration.

Table 3.3: Comparison of results for SOI = 350°

Scheme	IVC - SOC				SOC - EOC				EOC - EVO				TOTAL			
	I	N	IMEP	Δ	I	N	IMEP	Δ	I	N	IMEP	Δ	IMEP	Δ	$p_{\max}$	Δ
Ref			-5.737				10.968				1.446		6.728		57.025	
A	2	2	-5.714	-0.023	4	2	11.348	-0.380	2	2	1.603	-0.157	7.288	-0.560	53.961	3.064
B	3	3	-5.740	0.003	7	3	11.067	-0.099	3	3	1.473	-0.027	6.850	-0.123	56.834	0.191
C	4	4	-5.737	-0.000	8	4	10.994	-0.026	4	4	1.455	-0.009	6.763	-0.036	56.824	0.200
D	5	5	-5.737	-0.000	8	5	10.993	-0.025	5	5	1.453	-0.007	6.760	-0.032	56.888	0.137
E	6	5	-5.737	-0.000	10	5	10.984	-0.016	6	5	1.451	-0.005	6.748	-0.021	56.949	0.076

regions are reported for the different discretization schemes. The values of IMEP reported for the four macro-intervals should be interpreted as a "local" IMEP, i.e. the IMEP obtained restricting the pressure function to the considered domain. The global IMEP is also reported. Even the coarsest scheme A provides good accuracy levels in the region IVC - SOC, which means that a fine discretization in this interval is not needed. The schemes B still shows some small discrepancies with the reference solution but the results are acceptable, since the error in the total IMEP is lower than 2% and in the evaluation of $p_{\max}$ is much lower than 1%. The Schemes D and E show a very good agreement with the reference solution and very good results overall. If the target accuracy is not too demanding, scheme C provides a good compromise solution in terms of computation effort and accuracy. A similar behaviour is noticed for different engine operation point; results are reported in Appendix B.

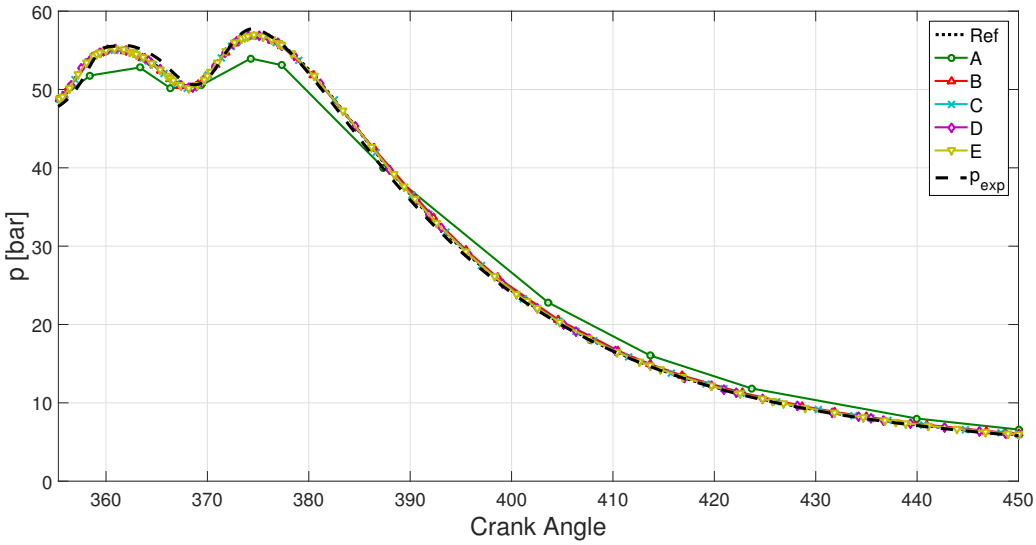

Figure 3.8: Pressure during combustion for different discretizations for SOI = 350°

4. Inverse problems

Accurate predictive models can also be used in order to estimate typical engine input parameters required to meet a given target in terms of MFB50 or IMEP, for example. This process requires the inversion of the proposed model and is usually a computationally expensive task. In the following we present some strategies that allow to solve the inverse problems with a high accuracy and a small computational cost.

4.0.1. MFB50

The inverse problem in this case means that we aim to determine the value of SOI that would result in a MFB50 value that equals a given target MFB50. The only parameter that can be changed is the SOI of the pilot injection, while all others remain fixed (that includes the time delay between the pilot and the main injection).

Let us assume for the moment that the values of τ_{pil} and τ_{main} are independent of SOI. With this in mind, the relationship between SOI and MFB50 for the model is:

$$\mathrm{MFB50}(\mathrm{SOI}) = \widehat{\mathrm{MFB50}} = \mathrm{MFB50}(\hat{\mathrm{SOI}}) + \Delta\theta,$$

where $\hat{\mathrm{SOI}}$ is any value of SOI for which we have solved the direct model (and obtained the corresponding MFB50) and $\Delta\theta = \mathrm{SOI} - \hat{\mathrm{SOI}}$. In other words, the only effect that a different SOI has on Q_{ch} (and therefore on MFB50) is to

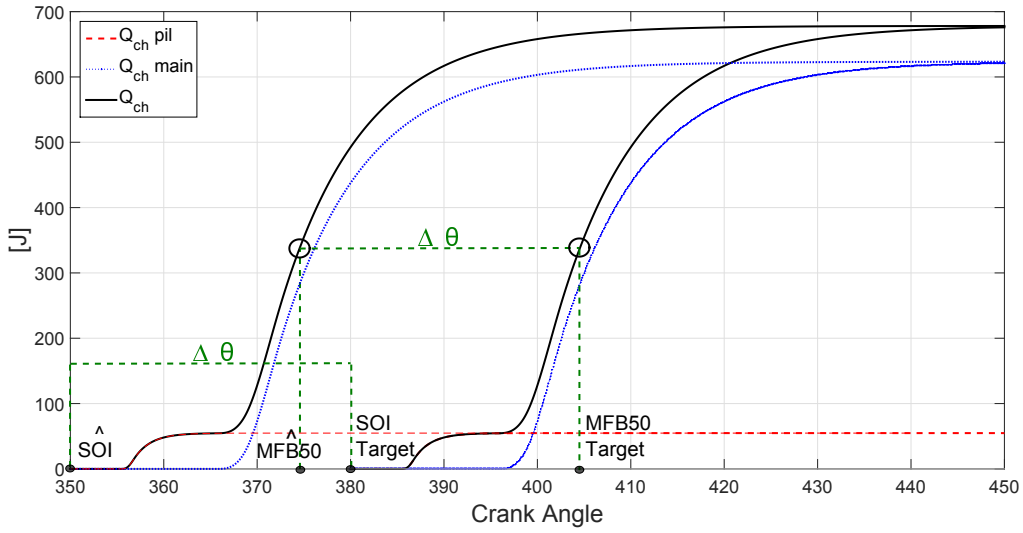

Figure 4.1: Obtaining the target SOI for a given target MFB50.

shift the curve left or right by the exact same magnitude as the difference in crank angle θ. Therefore, given a $\text{MFB50}_{\text{target}}$ and a value of start of injection $\hat{\text{SOI}}$ for which we have obtained MFB50 (as in the previous subsection), we have

$$\text{SOI}_{\text{target}} = \hat{\text{SOI}} + (\text{MFB50}_{\text{target}} - \hat{\text{MFB50}})$$

Where $\text{SOI}_{\text{target}}$ is the value of crank angle at which to start to injection so as to obtain $\text{MFB50}_{\text{target}}$. Figure 4.1 exemplifies this procedure.

redWe now consider the case where τ_{pil} and τ_{main} are a function of SOI, as described by functions (2.4) and (2.5). The curves obtained for the considered engine at 1500x5 operating point are reported in Figure 4.2. red The curves are extrapolated outside the range of applicability of equations (2.4)-(2.5) (extrapolated values are reported in thinner line in the Figure), in order to test the robustness of the method in providing a consistent solution also in computationally adverse configurations.

The problem now becomes an optimization problem, since now the relationship between Q_{ch} and SOI is more complicated than merely a shift in time (Figure 4.3). Nevertheless, we can overcome this issue by modifying our previous procedure and transforming it into an iterative method.

We begin by defining a tolerance *tol* and an interval I1 where we will look for our solution. The criteria used to define I1 was to rule out all values of SOI whose values of τ are such that the combustion begins after the value chosen and fixed to be the end of combustion. This procedure eliminates values of

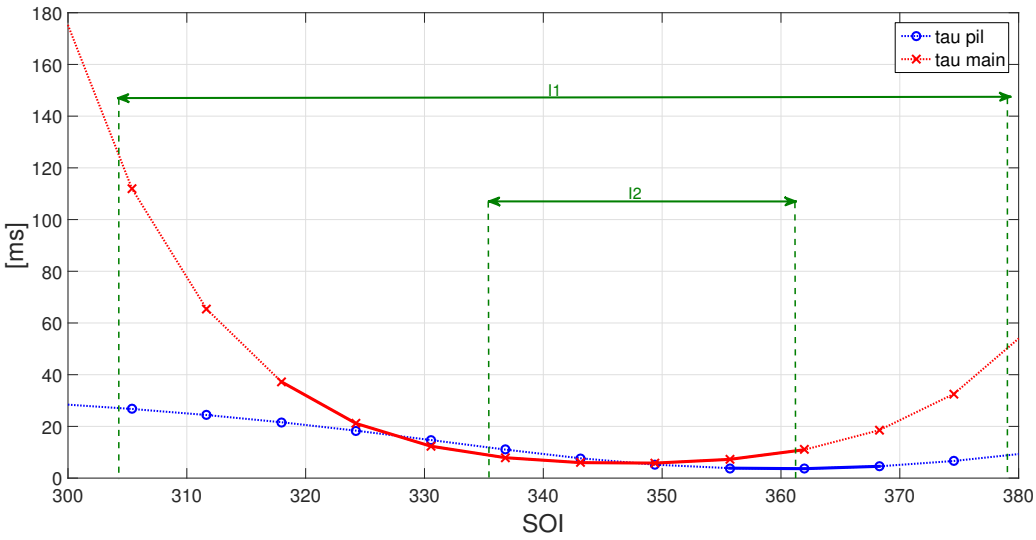

Figure 4.2: τ_{pil} and τ_{main} function of crank angle @1500x5 operating point.

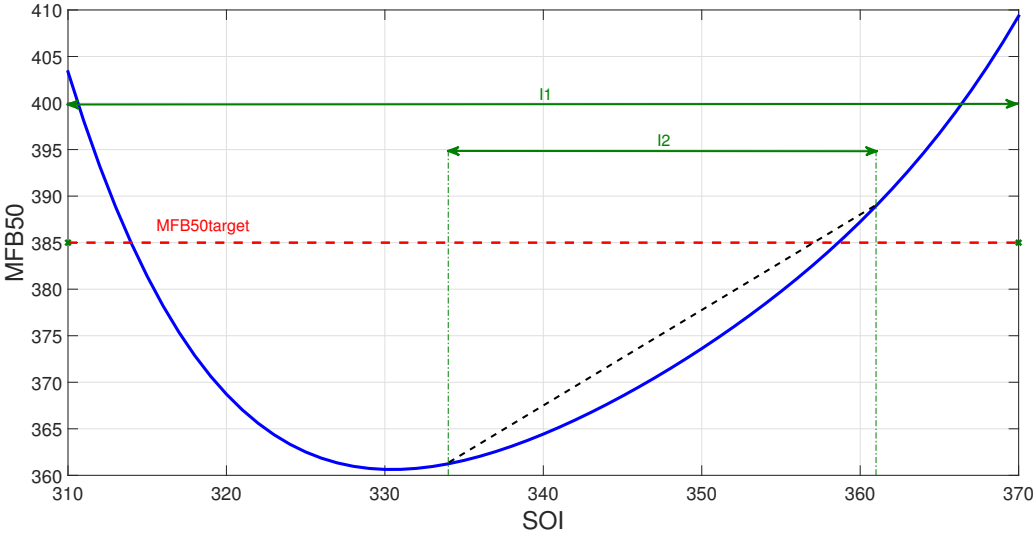

Figure 4.3: MFB50 as a function of SOI.

SOI very close to the EOC and also lower values of SOI corresponding to values of τ_{pil} and τ_{main} so large that the combustion begins much later than the injection and even after the EOC.

We define another interval, I2, that depends on τ_{pil} and τ_{main} and where the variation of these parameters is low enough such that we can approximate them as constants and then resort to a modified version of the procedure explained previously for constant τ_{pil} and τ_{main}. redWe remark that interval I2 contains the normal operational range. The iterative method that approximates the target SOI with variable injection delays is detailed as follows: we begin with an initial SOI_0 and its corresponding $\mathrm{MFB50}_0$. For each iteration we compute:

$$\begin{aligned} \Delta SOI &= \mathrm{MFB50}_{\mathrm{target}} - \mathrm{MFB50}_{\mathrm{k}}, \\ \Delta\tau &= \tau_{\mathrm{k}} - \tau_{\mathrm{k+1}}, \\ \mathrm{SOI}_{\mathrm{k+1}} &= \mathrm{SOI}_{\mathrm{k}} + \Delta SOI + \Delta\tau, \end{aligned}$$

where τ_{k} is the weighted sum of the values of τ_{pil} and τ_{main} for $\mathrm{SOI}_{\mathrm{k}}$ and $\tau_{\mathrm{k+1}}$ is the weighted sum of the values of τ_{pil} and τ_{main} for $\mathrm{SOI}_{\mathrm{k}} + \Delta SOI$ (which is an approximation of $\mathrm{SOI}_{\mathrm{k+1}}$). The respective weights of τ_{pil} and τ_{main} come from the percentage of total mass that is injected in the pilot and main in injection respectively. As long as these successive values of SOI remain inside I2, we continue with the iterations. If at some point we find a value close to $\mathrm{MFB50}_{target}$ for the chosen value of tol, the iteration ends. Otherwise, if we obtain a value $\mathrm{MFB50}_{\mathrm{k}}$ such that either

$$\begin{aligned} \mathrm{MFB50}_{\mathrm{k+1}} < \ & \mathrm{MFB50}_{target} \ < \mathrm{MFB50}_{\mathrm{k}} \\ & \text{or} \\ \mathrm{MFB50}_{\mathrm{k}} < \ & \mathrm{MFB50}_{target} \ < \mathrm{MFB50}_{\mathrm{k+1}} \end{aligned}$$

are true (in other words, if one value is above and the other one is below $\mathrm{MFB50}_{target}$), we will find the ultimate solution using the bisection method. redClearly the iterations within interval I2 are more efficient since only involve an evaluation of τ.

If we happen to be outside of interval I2 with our initial value, another method is used. This method is more computationally expensive that the one just described, but is used for values of $\mathrm{MFB50}_{target}$ outside standard engine operational ranges. A step-size $d\theta$ is chosen, controlling the accuracy of the iterative method described as follows: Starting at the right-end point of the interval I1 step $d\theta$ is performed to the left . At the corresponding SOI value, we compute the MFB50. If this new value of MFB50 is below our

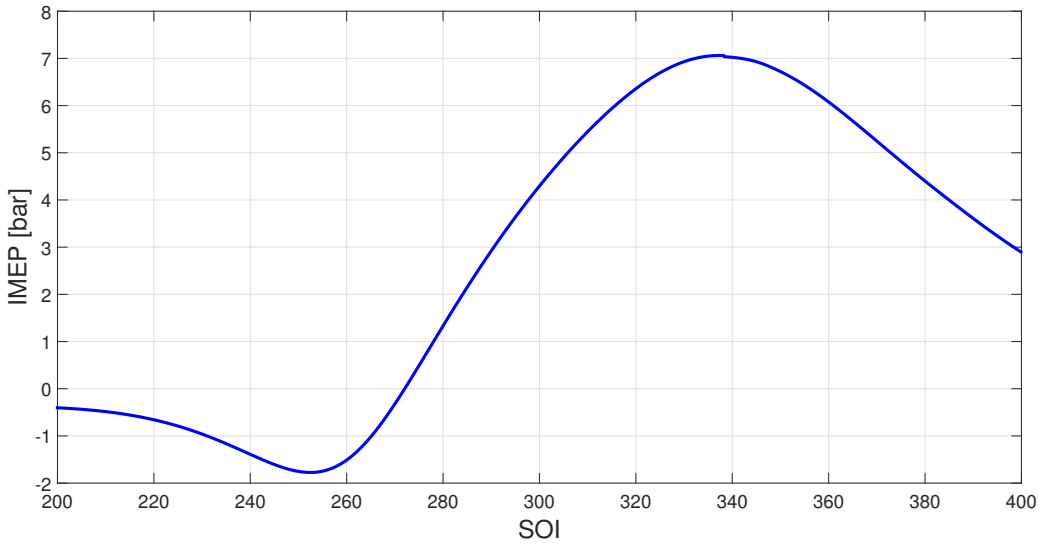

Figure 4.4: Example of a variation of IMEP with changing SOI

MFB50_{target}, it means that we have obtained the range where our solution is to be found. At this point, a linear interpolation will yield the desired value. The bisection method could also be used if more accuracy is required. If, instead, an MFB50 higher than the targer is evaluated a new step is performed. It is important to note that for values of MFB50 target that lie either below or above the curve, no solution for SOI can be found. The same thing may happen when the MFB50_{target} is very close to the minimum of the curve and could be bypassed if the precision is not high enough. In these cases, the returned value will be the one that gives the closest MFB50_{target} among those that were computed during the method.

4.0.2. IMEP

The aim of the optimization is to obtain the angle for the SOI of the pilot injection that produces the maximum IMEP, all other parameters remaining fixed. Since we do not have an explicit equation for IMEP, the procedure to find the maximum consists in solving the direct problem repeatedly for various values of SOI. An example of the curve of IMEP with varying SOI is shown in Figure 4.4. The results shown refer to the case of injection delay parameters independent from SOI. However, if variable parameters were considered, the application of the method would continue to be valid and only numerical values of IMEP would change.

The method used in this context is the golden section search. This technique finds the maximum by narrowing the range of values inside of the

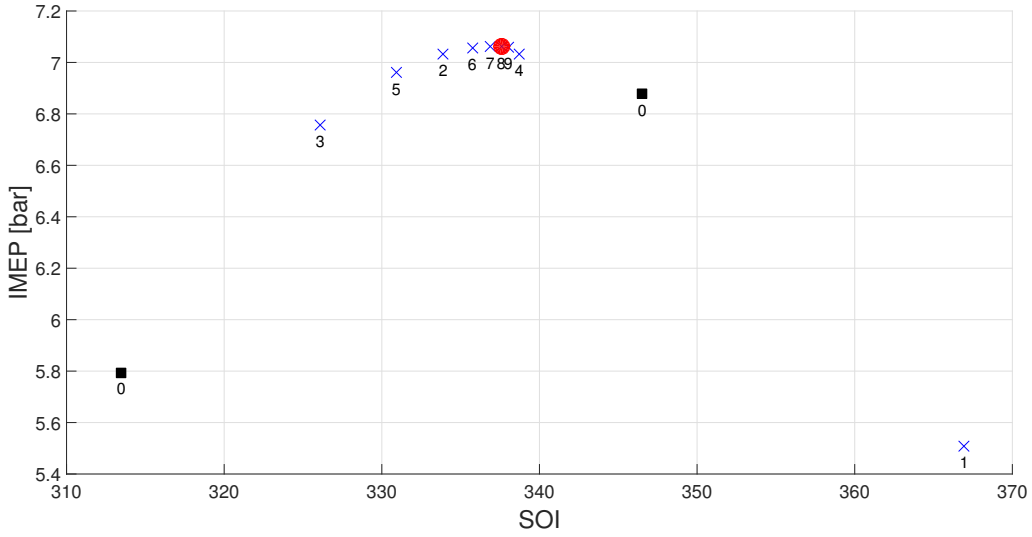

Figure 4.5: Iterations of the golden section search method.

interval where the maximum is known to exist. By iterating, we can achieve arbitrary accuracy of the solution, although the accuracy ultimately depends on how accurate we compute the IMEP at each step. We need to provide three initial values to the method, a, b and c, such that $a < b < c$ with $f(a) < f(b)$ and $f(c) < f(b)$. For the considered model we can define a as a value slightly larger than the IVC, c as a value smaller than EVO (but not too close to EVO that the combustion is cut short) and b as the average of a and c. The initial values as well as the successive approximations are shown in Figure 4.5 for the case under consideration. For a desired final accuracy of 2°, 9 iterations are required, although it can be seen from the figure that from iteration 6 the value for the current iteration is already close to the final result.

5. Some results about computational time

As mentioned before, computational cost and effectiveness of the proposed algorithm is the main focus of the present work. The proposed resolution strategies are, in fact, designed in order to keep the number of operation as low as possible, without compromising the general applicability of the method. In this section we report execution times for the described algorithms. It should be noted however that these values depend strongly on the computing performances of the hardware used and on the programming language chosen for the implementation. For solving the direct problem (as in sections 3.1, 3.2 and 3.3) we use a 0.1 degree target accuracy for MFB50,

Scheme "B" for the pressure profile and Gauss-Lobatto nodes for numerical integration. Times were computed using a commercial model laptop 64-bit Intel(R) Core(TM) i5-2430 CPU @ 2.40Gz. Results are shown in Table 5.1. redWe also include values of execution times using a commercial software for mathematical computations and a standard solving procedure i.e., solving everything numerically and using built-in functions of the software. Difference in time are orders of magnitude apart. A great amount of time is spent with the computation of MFB50 as expected, since the base methods require to obtain the values for Q_{ch} while our proposed algorithms start directly from an analytical solution.

Table 5.1: Execution time for the direct problem in ms

Method	MFB50	Pressure	IMEP	Total
Developed in this work	0.4	5.5	7.3	13.2
Commercial software	3000	2200	1400	6500

The execution time for the inverse problem of finding a target SOI given a target MFB50 is highly dependent of the value of the desired MFB50 target, and therefore special values were selected based on their position on the MFB50 - SOI curve (see Figure 4.3). The first iteration is always the same and agrees with the initial engine data. SOI target is computed to an accuracy of 0.5 degrees in crank angle. Table 5.2 lists the results, redwhich show the average execution time of a very large number of trials. It is seen that the best results are obtained when MFB50_{target} is about 365 (which corresponds to a SOI value of 340), which is within the usual operational range.

Table 5.2: Execution time for the inverse MFB50 problem

MFB50target	Characteristic	Time (ms)
355	Lower than the minimum	4.1
365	Begin of operating range	1.4
375	Middle of operating range	1.6
385	End of operating range	2.4
405	Slightly lower than the maximum value	7.5

Finally, for the optimization of IMEP we expect to obtain much higher execution times, since for every optimization we need to solve several direct problems. Table 5.3 shows the results.

Table 5.3: Execution time for the optimization of IMEP

Tolerance (CA)	Number of direct problems solved (N)	Time(T) (ms)	T/N
5	8	116.2	14.5
2	10	148.3	14.8
1	12	181.0	15.1
0.1	12	180.6	15.1

6. Conclusions

redIn this work an efficient numerical tool to evaluate key diesel engines combustion parameters is presented, based on a zero-dimensional model. The model is designed for model-based combustion control, through the prediction and the optimization of the MFB50, $p_{\max}$, and IMEP parameters. The novelty of the proposed approach lies in the analytical derivation of the equations describing the heat release rate Q_{ch} as a function of the SOI angle for the calculation and optimization of the MFB50, and in the use of customized numerical procedures for the combined resolution of the differential equations and the numerical integration for determining and optimizing the IMEP. The method is versatile since it allows for a very cost-efficient resolution without compromising the accuracy, but at the same time it can be used to obtain a very accurate solution if computation time is not an issue. The computation and optimization of the MFB50 can be performed in less than ten milliseconds with an accuracy of 0.5 degree in any operating condition, and the computation of the IMEP with a scheme providing an accuracy of about 2% and an optimization with respect to the SOI angle with an accuracy of 0.1 degree requires less than 0.2 s. The results obtained are promising for real-time response when implemented in an engine ECU.

Further improvements in performance are possible focusing on more optimized implementation and coding of the algorithms and on the programming language. Furthermore, by customizing the model for the application to one specific engine, many input data could be fixed and domains of interest could be bounded, thus leading to a faster execution.

Generalizations of the methods have already been surveyed (e.g. a higher number of injections, non-constant input data, different engine configurations) for the continuation of this work.

Acknowledgements

Authors are grateful to Ezio Spessa and Roberto Finesso for proving the experimental data and for many useful discussions and valuable suggestions. This work was supported by *Project "Idea" (56_RIJ13IDEA), Technology Platform in Automotive POR FESR 2007/2013* co-founded by Regione Piemonte.

References

[1] T. Johnson, Review of diesel emissions and control, SAE Int. J. Fuels Lubr 3 (2010) 16–29. doi:10.4271/2010-01-0301.

[2] M. Yao, Z. Zheng, H. Liu, Progress and recent trends in homogeneous charge compression ignition (HCCI) engines, Progress in Energy and Combustion Science 35 (2009) 398–437. doi:http://dx.doi.org/10.1016/j.pecs.2009.05.001.

[3] A. Carlucci, D. Laforgia, S. Motz, R. Saracino, S. Wenzel, Advanced closed loop combustion control of a LTC diesel engine based on in-cylinder pressure signals, Energy Conversion and Management 77 (0) (2014) 193 – 207. doi:http://dx.doi.org/10.1016/j.enconman.2013.08.054.

[4] E. Neshat, R. K. Saray, An optimized chemical kinetic mechanism for HCCI combustion of PRFs using multi-zone model and genetic algorithm, Energy Conversion and Management 92 (0) (2015) 172 – 183. doi:http://dx.doi.org/10.1016/j.enconman.2014.11.057.

[5] G. Cipolla, A. Vassallo, A. Catania, R. Spessa, C. Stan, L. Drischmann, Combined application of CFD modeling and pressure-based combustion diagnostics for the development of a low compression ratio high-performance diesel engine, SAE Technical Paper 2007-24-0034doi:10.4271/2007-24-0034.

[6] C. Beatrice, N. Rispoli, G. D. Blasio, G. Patrianakos, M. Kostoglou, A. Konstandopoulos, A. Imren, I. Denbratt, R. Palacin, Emission reduction technologies for the future low emission rail diesel engines: EGR vs SCR, SAE Technical Paper 2013-24-0087doi:10.4271/2013-24-0087.

[7] C. Guido, C. Beatrice, S. D. Iorio, P. Napolitano, D. B. G., A. Vassallo, C. Ciaravino, Assessment of closed-loop combustion control capability for biodiesel blending detection and combustion impact mitigation for an euro5 automotive diesel engine, SAE Technical Paper 2011-01-1193doi:10.4271/2011-01-1193.

[8] U. Asad, M. Zheng, Fast heat release characterization of a diesel engine, International Journal of Thermal Sciences 47 (12) (2008) 1688 – 1700. doi:http://dx.doi.org/10.1016/j.ijthermalsci.2008.01.009.

[9] F. Ponti, V. Ravaglioli, D. Moro, G. Serra, {MFB50} on-board estimation methodology for combustion control, Control Engineering Practice 21 (12) (2013) 1821 – 1829. doi:http://dx.doi.org/10.1016/j.conengprac.2013.05.001.

[10] F. Ponti, V. Ravaglioli, G. Serra, F. Stola, Instantaneous engine speed measurement and processing for mfb50 evaluation, SAE Int. J. Engines 2 (2) (2010) 235–244. doi:10.4271/2009-01-2747.

[11] V. Ravaglioli, D. Moro, G. Serra, F. Ponti, MFB50 on-board evaluation based on a zero-dimensional ROHR model, SAE Technical Paper 2011-01-1420doi:10.4271/2011-01-1420.

[12] O. Vitek, J. Macek, C. Poetsch, R. Tatschl, Modeling Cycle-to-Cycle Variations in 0-D/1-D simulation by means of combustion model parameter perturbations based on statistics of cycle-resolved data, SAE Int. J. Engines 6 (2) (2013) 1075–1098. doi:10.4271/2013-01-1314.

[13] N. Komninos, D. Hountalas, Improvement and validation of a multizone model for HCCI engine combustion concerning performance and emissions, Energy Conversion and Management 49 (10) (2008) 2530 – 2537. doi:http://dx.doi.org/10.1016/j.enconman.2008.05.008.

[14] N. S. Savva, D. T. Hountalas, Evolution and application of a pseudo-multi-zone model for the prediction of NOx emissions from large-scale diesel engines at various operating conditions, Energy Conversion and Management 85 (0) (2014) 373 – 388. doi:http://dx.doi.org/10.1016/j.enconman.2014.05.103.

[15] J. Asprion, O. Chinellato, L. Guzzella, Optimisation-oriented modelling of the NOx emissions of a diesel engine, Energy Conversion and Management 75 (0) (2013) 61 – 73. doi:http://dx.doi.org/10.1016/j.enconman.2013.05.039.

[16] U. Asad, J. Tjong, M. Zheng, Exhaust gas recirculation zero dimensional modelling and characterization for transient diesel combustion control, Energy Conversion and Management 86 (0) (2014) 309 – 324. doi:http://dx.doi.org/10.1016/j.enconman.2014.05.035.

[17] L. Lešnik, J. Iljaž, A. Hribernik, B. Kegl, Numerical and experimental study of combustion, performance and emission characteristics of a heavy-duty DI diesel engine running on diesel, biodiesel and their blends, Energy Conversion and Management 81 (0) (2014) 534 – 546. doi:http://dx.doi.org/10.1016/j.enconman.2014.02.039.

[18] S. Soylu, Examination of combustion characteristics and phasing strategies of a natural gas HCCI engine, Energy Conversion and Management 46 (1) (2005) 101 – 119. doi:http://dx.doi.org/10.1016/j.enconman.2004.02.013.

[19] J. Chung, S. Oh, K. Min, M. Sunwoo, Real-time combustion parameter estimation algorithm for light-duty diesel engines using in-cylinder pressure measurement, Applied Thermal Engineering 60 (12) (2013) 33 – 43. doi:http://dx.doi.org/10.1016/j.applthermaleng.2013.06.003.

[20] C. Guardiola, J. Lpez, J. Martn, D. García-Sarmiento, Semiempirical in-cylinder pressure based model for NOX prediction oriented to control applications, Applied Thermal Engineering 31 (16) (2011) 3275 – 3286. doi:http://dx.doi.org/10.1016/j.applthermaleng.2011.05.048.

[21] A. Catania, S. Finesso, R. Spessa, G. Cipolla, A. Vassallo, Combustion system optimization of a low compression-ratio PCCI diesel engine for light-duty application, SAE Int. J. Engines 2 (1) (2009) 1314 – 1326. doi:10.4271/2009-01-1464.

[22] R. Finesso, D. Misul, E. Spessa, Development and validation of a semi-empirical model for the estimation of particulate matter in diesel engines, Energy Conversion and Management 84 (0) (2014) 374 – 389. doi:http://dx.doi.org/10.1016/j.enconman.2014.04.053.

[23] J. A. Caton, The thermodynamic characteristics of high efficiency, internal-combustion engines, Energy Conversion and Management 58 (0) (2012) 84 – 93. doi:http://dx.doi.org/10.1016/j.enconman.2012.01.005.

[24] J. A. Caton, Combustion phasing for maximum efficiency for conventional and high efficiency engines, Energy Conversion and Management 77 (0) (2014) 564 – 576. doi:http://dx.doi.org/10.1016/j.enconman.2013.09.060.

[25] R. Finesso, E. Spessa, A real time zero-dimensional diagnostic model for the calculation of in-cylinder temperatures, HRR and nitrogen oxides in diesel engines, Energy Conversion and Management 79 (0) (2014) 498 – 510. doi:http://dx.doi.org/10.1016/j.enconman.2013.12.045.

[26] A. E. Catania, R. Finesso, E. Spessa, Predictive zero-dimensional combustion model for di diesel engine feed-forward control, Energy Conversion and Management 52 (2011) 3159–3175. doi:http://dx.doi.org/10.1016/j.enconman.2011.05.003.

[27] A. E. Catania, R. Finesso, E. Spessa, A. Catanese, L. Gerhard, Combustion prediction by a low-throughput model in modern diesel engines, SAE Int. J. Engines 4 (2011) 2106–2123. doi:10.4271/2011-01-1410.

[28] R. Finesso, E. Spessa, Real-time predictive modeling of combustion and nox formation in diesel engines under transient conditions, SAE Technical Paper 2012-01-0899. doi:10.4271/2012-01-0899.

[29] A. E. Catania, R. Finesso, E. Spessa, Assessment of a low-throughput predictive model for indicated cycle, combustion noise and nox calculation in diesel engines in steady state and transient operations, 2012 Spring Technical Conference of the ASME Internal Combustion Engine Division, Torino (Italy), May 6-9 (2012) 273–288doi:10.1115/ICES2012-81094.

[30] R. Finesso, E. Spessa, Ignition delay prediction of multiple injections in diesel engines, Fuel 119 (0) (2014) 170 – 190. doi:http://dx.doi.org/10.1016/j.fuel.2013.11.040.

[31] R. Finesso, E. Spessa, A feed-forward approach for the real-time estimation and control of MFB50 and SOI in diesel engines, SAE Int. J. Engines 7 (1) (2014) 528–549. doi:10.4271/2014-01-9046.

[32] C. Ericson, B. Westerberg, M. Andersson, R. Egnell, Modelling diesel engine combustion and nox formation for model based control and simulation of engine and exhaust aftertreatment systems, SAE Technical Paper 2006-01-0687doi:10.4271/2006-01-0687.

[33] L. Jongsuk, O. Seungsuk, C. Jeasung, M. Sunwoo, Real-time combustion phase detection using central normalized difference pressure in CRDI diesel engines, J. Eng. Gas Turbines Power 134 (8) (2012) 082801. doi:10.1115/1.4006582.

[34] H. Husted, D. Kruger, G. Fattic, G. Ripley, E. Kelly, Cylinder pressure-based control of pre-mixed diesel combustion, SAE Technical Paper 2007-01-0773doi:10.4271/2007-01-0773.

[35] E. Corti, C. Forte, A statistical approach to spark advance mapping, J. Eng. Gas Turbines Power 132 (8) (2010) 082803. doi:10.1115/1.4000294.

[36] W. Northrop, S. Bohac, D. Assanis, Premixed low temperature combustion of biodiesel and blends in a high speed compression ignition

engine, SAE Int. J. Fuels Lubr. 2 (1) (2009) 28–40. doi:10.4271/2009-01-0133.

[37] J. Arrègle, J. López, J. García, C. Fenollosa, Development of a zero-dimensional diesel combustion model. part 1: Analysis of the quasi-steady diffusion combustion phase, Applied Thermal Engineering 23 (11) (2003) 1301 – 1317. doi:http://dx.doi.org/10.1016/S1359-4311(03)00079-6.

[38] J. Arrègle, J. López, J. García, C. Fenollosa, Development of a zero-dimensional diesel combustion model: Part 2: Analysis of the transient initial and final diffusion combustion phases, Applied Thermal Engineering 23 (11) (2003) 1319 – 1331. doi:http://dx.doi.org/10.1016/S1359-4311(03)00080-2.

[39] U. Demir, N. Yilmaz, G. Coskun, H. S. Soyhan, Evaluation of zero dimensional codes in simulating IC engines using primary reference fuel, Applied Thermal Engineering 76 (0) (2015) 18 – 24. doi:http://dx.doi.org/10.1016/j.applthermaleng.2014.10.084.

Appendix A. Analytical expression for Q_{ch}

Given a triangular injection profile, characterized by a start of injection (SOI) angle, an end of injection (EOI) angle and a maximum injection rate $M_{\max}$, it is possible to derive an analytical expression for Q_{ch} and consequently for Q_{net}. Computations are performed independently for each injection pulse, thus obtaining $Q_{\mathrm{ch,i}}$ for $j = 1...n$, with n being the total number of injections (usually 1,2 or 3) and subsequently setting $Q_{\mathrm{ch}} = \sum_{j=1}^{n} Q_{\mathrm{ch,j}}$. Consequently the procedure for one injection is shown, and the pulse index j is dropped from all the equations. Furthermore, all calculations are done considering the crank angle θ as the independent variable instead of time (a simple linear function transforms time t into θ).

The injection rate, is described as follows:

$$m(\theta) = \begin{cases} 0 & \theta < \theta_{\mathrm{soi}} \\ \dfrac{1000 M_{\max}(\theta - \theta_{\mathrm{soi}})}{3N(\theta_{\mathrm{eoi}} - \theta_{\mathrm{soi}})} & \theta_{\mathrm{soi}} \leq \theta < \dfrac{\theta_{\mathrm{eoi}} + \theta_{\mathrm{soi}}}{2} \\ \dfrac{1000 M_{\max}(\theta_{\mathrm{eoi}} - \theta)}{3N(\theta_{\mathrm{eoi}} - \theta_{\mathrm{soi}})} & \dfrac{\theta_{\mathrm{eoi}} + \theta_{\mathrm{soi}}}{2} \leq \theta < \theta_{\mathrm{eoi}} \\ 0 & \theta_{\mathrm{eoi}} \leq \theta \end{cases}$$

The quantity Q_{fuel} is defined according to (2.2)-(2.3) as:

$$Q_{\text{fuel}}(\theta) = \begin{cases} 0 & \theta < \theta_{\text{soi}} \\ \dfrac{500 H_{\text{i}} M_{\max}(\theta - \theta_{\text{soi}})^2}{3N(\theta_{\text{eoi}} - \theta_{\text{soi}})} & \theta_{\text{soi}} \le \theta < \dfrac{\theta_{\text{eoi}} + \theta_{\text{soi}}}{2} \\ \dfrac{250 H_{\text{i}} M_{\max}\left(2\theta^2 - 4\theta\theta_{\text{eoi}} + \theta_{\text{eoi}}^2 + 2\theta_{\text{eoi}}\theta_{\text{soi}} - \theta_{\text{soi}}^2\right)}{3N(\theta_{\text{eoi}} - \theta_{\text{soi}})} & \dfrac{\theta_{\text{eoi}} + \theta_{\text{soi}}}{2} \le \theta < \theta_{\text{eoi}} \\ \dfrac{250 H_{\text{i}} M_{\max}(\theta_{\text{eoi}} - \theta_{\text{soi}})}{3N} & \dfrac{\theta_{\text{eoi}} + \theta_{\text{soi}}}{2} \le \theta < \theta_{\text{eoi}} \end{cases}$$

The expression of Q_{ch} for one injection is then obtained solving (2.1). Setting:

$$\begin{aligned} \phi &= (-3KN\theta_{\text{eoi}} + 3KN\theta_{\text{soi}})/(18N^2(\theta_{\text{eoi}} - \theta_{\text{soi}})) \\ \varphi &= (\tau + \theta_{\text{soi}})\phi \\ \psi &= (\tau + (\theta_{\text{eoi}} - \theta_{\text{soi}})/2 + \theta_{\text{soi}})\phi \\ \varsigma &= (\tau + \theta_{\text{eoi}})\phi \end{aligned}$$

we obtain the piecewise-defined function as detailed below.

- For $\theta < \tau + \theta_{\text{soi}}$,

$$Q_{\text{ch}}(\theta) = 0$$

- For $\tau + \theta_{\text{soi}} \le \theta$ and $\theta < \tau + (\theta_{\text{eoi}} - \theta_{\text{soi}})/2 + \theta_{\text{soi}}$,

$$\begin{aligned} Q_{\text{ch}}(\theta) = {} & \left(3K^2N(\theta_{\text{eoi}} - \theta_{\text{soi}})e^{\varphi}\right)^{-1}(500 H_{\text{i}} M_{\max}(72N^2(e^{\varphi} - e^{\theta\phi}) + e^{\varphi}(12KN\tau + K^2\tau^2 \\ & -12KN\theta - 2K^2\tau\theta + K^2\theta^2 + 12KN\theta_{\text{soi}} + 2K^2\tau\theta_{\text{soi}} - 2K^2\theta\theta_{\text{soi}} + K^2\theta_{\text{soi}}^2))) \end{aligned}$$

- For $\tau + (\theta_{\text{eoi}} - \theta_{\text{soi}})/2 + \theta_{\text{soi}} \le \theta$ and $\theta < \tau + \theta_{\text{eoi}}$

$$\begin{aligned} Q_{\text{ch}}(\theta) = {} & \left(3K^2N(\theta_{\text{eoi}} - \theta_{\text{soi}})\right)^{-1}(-250e^{-(\varphi+\psi)}H_i M_{max}(-288N^2e^{\theta\phi+\varphi} \\ & +144N^2e^{\theta\phi+\psi}) + 144N^2 + 24KN\tau + 2K^2\tau^2 - 24KN\theta \\ & -4K^2\tau\theta + 2K^2\theta^2 + 24KN\theta_{\text{eoi}} + 4K^2\tau\theta_{\text{eoi}} - 4K^2\theta\theta_{\text{eoi}} + K^2\theta_{\text{eoi}}^2 \\ & +2K^2\theta_{\text{eoi}}\theta_{\text{soi}} - K^2\theta_{\text{soi}}^2) \end{aligned}$$

- For $\tau + \theta_{\text{eoi}} \le \theta$

$$\begin{aligned} Q_{\text{ch}}(\theta) = {} & \left(3K^2N(\theta_{\text{eoi}} - \theta_{\text{soi}})\right)^{-1}(250 H_{\text{i}} M_{\max} e^{-(K\theta)/(6N) - \varsigma - \varphi - \psi}(144N^2(2e^{\varsigma+\varphi} \\ & -e^{\varsigma+\psi} - e^{\varphi+\psi})) + K^2\theta_{\text{eoi}}^2 - 2K^2\theta_{\text{eoi}}\theta_{\text{soi}} + K^2\theta_{\text{soi}}^2) \end{aligned}$$

Appendix B. IMEP computation results

In the following we present results for other engine operation points so as to show that the procedures we have developed can be extended to different configurations.

Table B.1: Comparison of results @1500x2 engine point

Scheme	IVC - SOC				SOC - EOC				EOC - EVO				TOTAL			
	I	N	IMEP	Δ	I	N	IMEP	Δ	I	N	IMEP	Δ	IMEP	Δ	p_{max}	Δ
Ref			-4.682				7.256				0.907		3.446		43.718	
A	2	2	-4.720	0.038	4	2	7.355	-0.099	2	2	0.983	-0.076	3.584	-0.138	41.572	2.146
B	3	3	-4.684	0.001	7	3	7.281	-0.025	3	3	0.920	-0.013	3.483	-0.037	43.068	0.650
C	4	4	-4.682	-0.000	8	4	7.268	-0.012	4	4	0.912	-0.005	3.464	-0.017	43.567	0.151
D	5	5	-4.682	-0.000	8	5	7.261	-0.005	5	5	0.910	-0.003	3.455	-0.008	43.598	0.120
E	6	5	-4.682	-0.000	10	5	7.265	-0.010	6	5	0.910	-0.003	3.459	-0.013	43.584	0.133

Table B.2: Comparison of results @2000x2 engine point

Scheme	IVC - SOC				SOC - EOC				EOC - EVO				TOTAL			
	I	N	IMEP	Δ	I	N	IMEP	Δ	I	N	IMEP	Δ	IMEP	Δ	p_{max}	Δ
Ref			-4.855				7.600				0.984		3.652		46.979	
A	2	2	-4.836	-0.019	4	2	7.553	0.047	2	2	1.043	-0.058	3.683	-0.031	44.724	2.255
B	3	3	-4.858	0.003	7	3	7.668	-0.067	3	3	1.003	-0.019	3.735	-0.083	46.446	0.533
C	4	4	-4.855	0.000	8	4	7.614	-0.014	4	4	0.990	-0.006	3.671	-0.019	46.825	0.154
D	5	5	-4.855	0.000	8	5	7.610	-0.010	5	5	0.988	-0.004	3.666	-0.014	46.853	0.125
E	6	5	-4.855	0.000	10	5	7.605	-0.004	6	5	0.987	-0.002	3.658	-0.007	46.884	0.095

Table B.3: Comparison of results @2000x5

Scheme	IVC - SOC				SOC - EOC				EOC - EVO				TOTAL			
	I	N	IMEP	Δ	I	N	IMEP	Δ	I	N	IMEP	Δ	IMEP	Δ	p_{max}	Δ
Ref			-6.260				11.542				1.592		6.812		63.291	
A	2	2	-6.210	-0.050	4	2	11.503	0.039	2	2	1.694	-0.102	6.925	-0.113	61.141	2.150
B	3	3	-6.261	0.002	7	3	11.677	-0.136	3	3	1.624	-0.032	6.978	-0.166	62.810	0.481
C	4	4	-6.260	-0.000	8	4	11.566	-0.024	4	4	1.601	-0.009	6.846	-0.034	63.083	0.208
D	5	5	-6.260	0.000	8	5	11.565	-0.024	5	5	1.599	-0.007	6.843	-0.031	63.165	0.126
E	6	5	-6.260	0.000	10	5	11.553	-0.012	6	5	1.596	-0.004	6.828	-0.016	63.174	0.117

Table B.4: Comparison of results @2500x8 engine point

Scheme	IVC - SOC				SOC - EOC				EOC - EVO				TOTAL			
	I	N	IMEP	Δ	I	N	IMEP	Δ	I	N	IMEP	Δ	IMEP	Δ	p_{max}	Δ
Ref			-7.914				16.248				2.435		10.455		99.465	
A	2	2	-7.873	-0.041	4	2	17.334	-1.085	2	2	2.769	-0.333	11.915	-1.460	95.334	4.131
B	3	3	-7.914	0.000	7	3	16.397	-0.149	3	3	2.478	-0.042	10.646	-0.191	98.643	0.822
C	4	4	-7.914	0.000	8	4	16.319	-0.070	4	4	2.454	-0.019	10.544	-0.089	99.253	0.213
D	5	5	-7.914	0.000	8	5	16.297	-0.049	5	5	2.449	-0.013	10.517	-0.062	99.218	0.247
E	6	5	-7.914	0.000	10	5	16.283	-0.034	6	5	2.445	-0.009	10.498	-0.043	99.302	0.163

Table B.5: Comparison of results @2750x12 engine point

Scheme	IVC - SOC				SOC - EOC				EOC - EVO				TOTAL			
	I	N	IMEP	Δ	I	N	IMEP	Δ	I	N	IMEP	Δ	IMEP	Δ	p_{max}	Δ
Ref			-8.327				19.908				3.171		14.409		120.359	
A	2	2	-8.296	-0.032	4	2	20.441	-0.533	2	2	3.450	-0.279	15.253	-0.844	112.311	8.049
B	3	3	-8.328	0.000	7	3	20.055	-0.147	3	3	3.217	-0.046	14.601	-0.193	119.712	0.648
C	4	4	-8.328	0.000	8	4	19.951	-0.043	4	4	3.187	-0.016	14.468	-0.060	119.872	0.488
D	5	5	-8.328	0.000	8	5	19.946	-0.038	5	5	3.184	-0.013	14.459	-0.051	119.997	0.363
E	6	5	-8.327	0.000	10	5	19.928	-0.020	6	5	3.179	-0.008	14.437	-0.028	120.116	0.244

The results show that the procedure can be extended to other conditions and as in the example case, scheme C shows a very good approximation with

a reasonable cost. In some cases, even scheme B is accurate enough and even less costly.